ICSV13 - Vienna
The Thirteenth International Congress on Sound and Vibration
Vienna, Austria, July 2-6, 2006

Control algorithms for semi–active vibration control of mechanical structures with adaptive friction dampers

Jens Becker* and Lothar Gaul

Institute of Applied and Experimental Mechanics, University of Stuttgart,
Pfaffenwaldring 9, 70569 Stuttgart
j.becker@iam.uni-stuttgart.de, gaul@iam.uni-stuttgart.de

Abstract

Reduction of structural vibrations are of major interest in mechanical engineering for lowering sound emission of vibrating structures, improving accuracy of machines and increasing structure durability. Besides optimal passive design, this problem can be tackled by structural vibration control concepts, which become more and more important as lightweight constructions evolve. In this contribution, a semi–active control concepts for the adaptive control of the normal force of friction dampers attached to a vibrating structure are presented. In contrast to purely active control strategies, semi-active control algorithms have the advantage of yielding intrinsically stable closed–loop systems and low energy consumption. In this work, the normal force applied to the frictional interfaces between structure and damper elements is applied by piezoelectric stack actuators and controlled accordingly to the measured structural vibrations for optimal damping. The control design is based on simplified finite–element models of the structural dynamics. Experimental results for a test structure are presented.

1 Introduction

Semi–active control strategies in structural vibration control offer various advantages compared to passive measures of vibration reduction and active vibration control (AVC). Hereby semi–active means, that the passive properties of damping elements are actively controlled. From this it follows that semi–active control in contrast to AVC feeds no energy into the structure under control. This in turn eliminates the important problem of system destabilization due to spillover effects which often limits the applicability of AVC of flexible structures [1, 2]. Hence, semi–active control concepts yield guaranteed stable closed–loop systems. On the other hand, because semi–active control concepts rely generally on passive damping mechanisms, the maximal achievable damping is limited. Though, they outperform passive vibration reduction means due to the ability to adapt to the instantaneous vibration state of the structure.

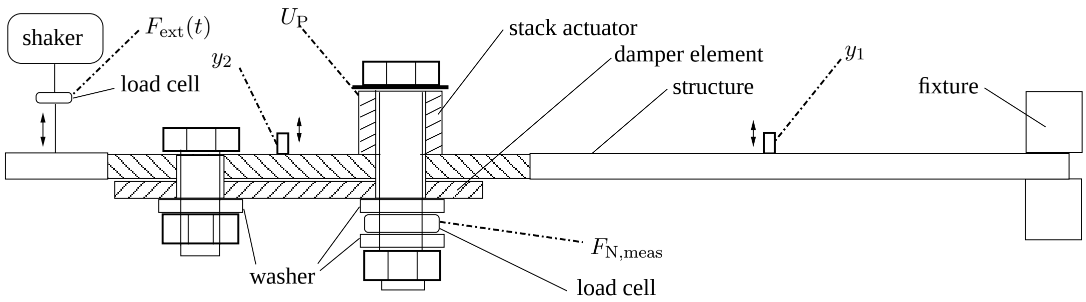

Figure 1: Experimental setup of the investigated structure with adaptive friction dampers (amplifiers are not shown for sake of clarity).

property	beam	damper
length	775 mm	160 mm
width	40 mm	40 mm
thickness	3 mm	3 mm
material	steel	steel

manufacturer	PI ceramics
type	306.20
maximum displacement	20 μm
stiffness	180 N/μm
operating voltage	-750 V .. 250 V

Table 1: Properties of structure and piezoelectric stack actuator (cf. with Fig. 1).

Therefore, semi–active structural control is related to the context of adaptive structures. The idea of using friction in joints to damp structural vibrations by semi–active normal force control can be found in [3, 4]. Hereby, only discrete joints and idealized structures are considered. The concept of semi–active control is most popular in the context of magnetorheological or electrorheological dampers and variable–stiffness dampers, see e.g. [5, 6]. In this contribution, strategies for the semi–active control of the applied normal force on frictional interfaces between a beam structure and an added damper element are investigated in order to optimally damp structural. Experiments are conducted with a test structure depicted in Fig. 1. The attached friction damper is fixed on it left side to the beam structure by a high clamping force whereas the normal force can be controlled on the other side.

2 Semi–active Vibration Control

Experimental investigations of structures with joints have shown that relatively simple dynamical friction models are capable to model the dominant effects [7]. From experiments, e.g. see [8], the Masing model shown in Fig. 2 has proven its usability for bolted joints. From this discrete models, two control strategies are derived in the following.

2.1 Hysteresis–optimal Control

For the adaptive damping of structural vibrations, only approximately mono–frequent excitations are considered, which represents no limitation in most applications. Additionally, it is assumed that the dominant damping effects originate from the contact area below the normal force actuator. A discrete friction model captures the dominant effects. Then, the frictional

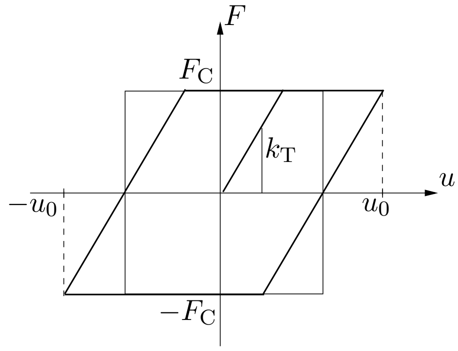

Figure 2: Hysteresis for Coulomb and Masing friction model with tangential stiffness k_T.

work W_d during one vibration cycle is maximized. This corresponds to maximizing the enclosed hysteresis area, hence the resulting control law is shortly denoted as hysteresis–optimal control. The normal force that maximizes the dissipated work W_d can be determined off-line with respect to the friction model parameters and the vibration amplitude. For the Masing model (see Fig. 2), the dissipated energy per cycle evaluates to

$$W_\mathrm{d} = 4\left(u_0 - \frac{F_\mathrm{C}}{k_\mathrm{T}}\right) F_\mathrm{C} \quad \text{with} \quad F_\mathrm{C} = \mu\, F_\mathrm{N}. \tag{1}$$

Maximizing W_d yields the optimal normal force F_N as function of the tangential contact stiffness k_T, the friction coefficient μ and the amplitude of the relative sliding oscillation amplitude u_0,

$$F_\mathrm{N} = f(u_0) = \frac{k_\mathrm{T}\, u_0}{2\mu}. \tag{2}$$

The expression (2) can now be used to derive a control algorithm. First, the vibration amplitude must be estimated from vibration measurements which are performed in this contribution by accelerometers. The relative displacement beneath the actuator is estimated by a modal filter whose inputs are the twice integrated measured accelerations $\boldsymbol{y}_\mathrm{meas}(t)$,

$$\hat{\boldsymbol{x}} = \boldsymbol{C}_\mathrm{meas}^{-1} \int_0^t \int_0^t \boldsymbol{y}_\mathrm{meas} \mathrm{dt}\ \mathrm{dt}, \qquad \hat{\mathrm{u}} = \boldsymbol{c}_\mathrm{rel}^\mathrm{T}\, \hat{\boldsymbol{x}}. \tag{3}$$

Hereby the inverse matrix $\boldsymbol{C}_\mathrm{meas}^{-1}$ represents the modal analyzer and $\boldsymbol{c}_\mathrm{rel}^\mathrm{T}$ represents the modal synthesizer (or output matrix) for the relative displacement; for details of the classical independent modal control see [2]. All matrices are derived from a finite–element (FE) model for the linear limit case without friction. The FE model parameters are updated by experimental modal analysis of the test structure. Altogether, this model–based approach allows the efficient estimation of non–measureable relative movements. Note that for each mode to be controlled, at least one sensor must be used. From this, the actual vibration amplitude is estimated by

$$\hat{u}_0(t) \approx \frac{\pi}{2T} \int_{t-T}^{t} |\hat{u}(t)|\ \mathrm{dt}. \tag{4}$$

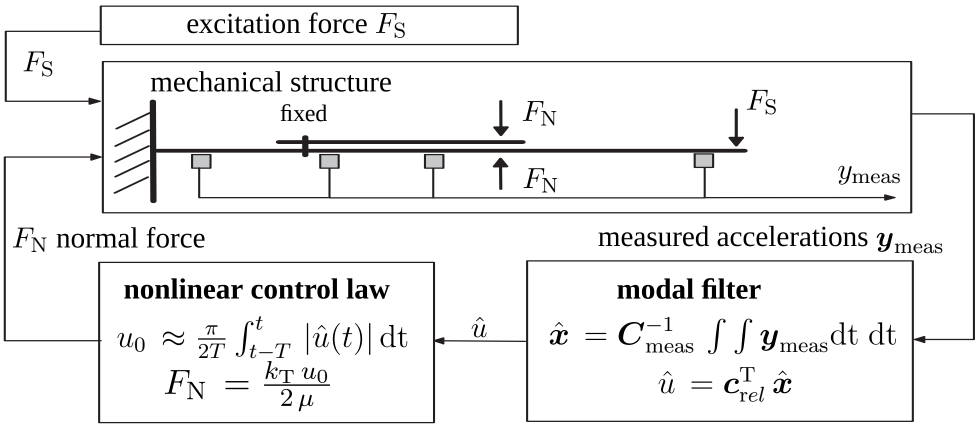

Figure 3: Closed control loop schematic of the proposed hysteresis–optimal control law.

Note that for this, the signal $u(t)$ must have zero mean, which is fullfilled due to the use of accelerometers. For sensors with static components, the mean value must be treated similar to (4) and subtracted in the integral.

Because the integral evaluation needs large memory to store the signal $\hat{u}(t)$ for $[t-T, t]$ for a reasonable integration time T much bigger than the vibration period, (4) is approximated for efficient implementation by a PT_1 element according to

$$T_0 \, \dot{\hat{u}}_0(t) + \hat{u}_0(t) = \frac{\pi}{2} |\hat{u}(t)|. \tag{5}$$

Hereby, the time constant T_0 prescribes how fast the controller reacts to a change in the amplitude. The obtained closed loop is depicted in Fig. 3.

2.2 Lyapunov–type Control

In [4], a Lyapunov function method is used to derive an optimal control law from the discrete friction model. If the Masing friction model is used for the derivation, the obtained control law depends on the friction force, which is not measureable or observeable for the investigated test structure. Hence the Coulomb model is used which approximates well the Masing model for high tangential stiffness values k_T and yields the control law (6). Using the Lyapunov design procedure for the Coulomb friction model, the derived control law is a velocity–dependent bang–bang controller. Because the bang–bang behavior leads to chatter, it is regularized with a boundary layer ϵ yielding

$$F_N = \begin{cases} F_{N,min} \left(1 - \frac{|\dot{u}|}{\epsilon}\right) + F_{N,max} \frac{|\dot{u}|}{\epsilon} & \text{for} \quad |\dot{u}| < \epsilon \\ F_{N,max} & \text{for} \quad |\dot{u}| \geq \epsilon \end{cases} \tag{6}$$

The relative tangential velocity in the interface beneath the normal force actuator is estimated in an similar way to (3). Note that in the case of piezoelectric actuators, the minimal and

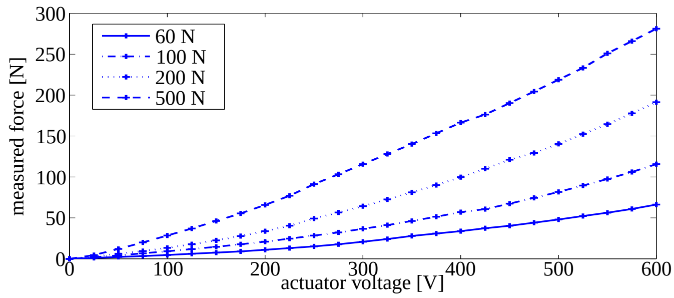

Figure 4: Measured stroke of the stack actuator for different preclamping forces.

maximal normal forces $F_{\mathrm{N,min}}$ and $F_{\mathrm{N,max}}$ are determined by the mechanical properties of the actuator configuration.

3 Experimental Results

The proposed control laws are implemented and experimentally investigated for a beam–like test structure depicted in Fig. 1 with properties given in Tab. 1. For the modal filter, four accelerometers are attached to the structure, hence the first four modes are included in the relative displacement estimation and can be controlled. The control algorithms are implemented on a *LabView PXI* real–time system running at 5 kHz.

3.1 Normal Force Actuator

For application of the normal force, a hollow piezoelectric stack actuator clamped by a bolt is used as shown in Fig. 1 (technical data are given Tab. 1). The applied normal force is measured by a strain–gage based load cell sensor, that allows measuring static force signal components, which is essential for this application. Hereby, the maximum achieveable actuator force stroke depends on the stiffness of the clamping and the actuator stiffness itself. Details of modeling of piezoelectric materials can be found in [2]. Note that the actuator block force of 3600 N is only theoretically obtained for infinite clamping stiffness, i.e. zero displacement. Hence, the force–voltage dependency for different clamping forces applied by tightening of the screw must be determined experimentally. One example of such a measurement is presented in Fig. 4. The measurements clearly reveal a nonlinear stiffness of the structure in normal direction depending on the clamping normal force. This effect is mainly due to the multiple contact pairs introduced between the screw, force measurement cell, washers, the structure but also some nonlinearities for high–voltage operation of the piezoelectric stack actuator come into play. This nonlinear relation makes an underlying control of the applied normal force for the hysteresis–optimal control necessary, which is performed by a proportional-integral (PI) controller that controls the applied normal force F_{N} given from the hysteresis–optimal control law. Because the Lyapunov–type control possesses very high dynamics, a underlaying PI control would be too slow for high frequencies. Therefore a correction based on the force–

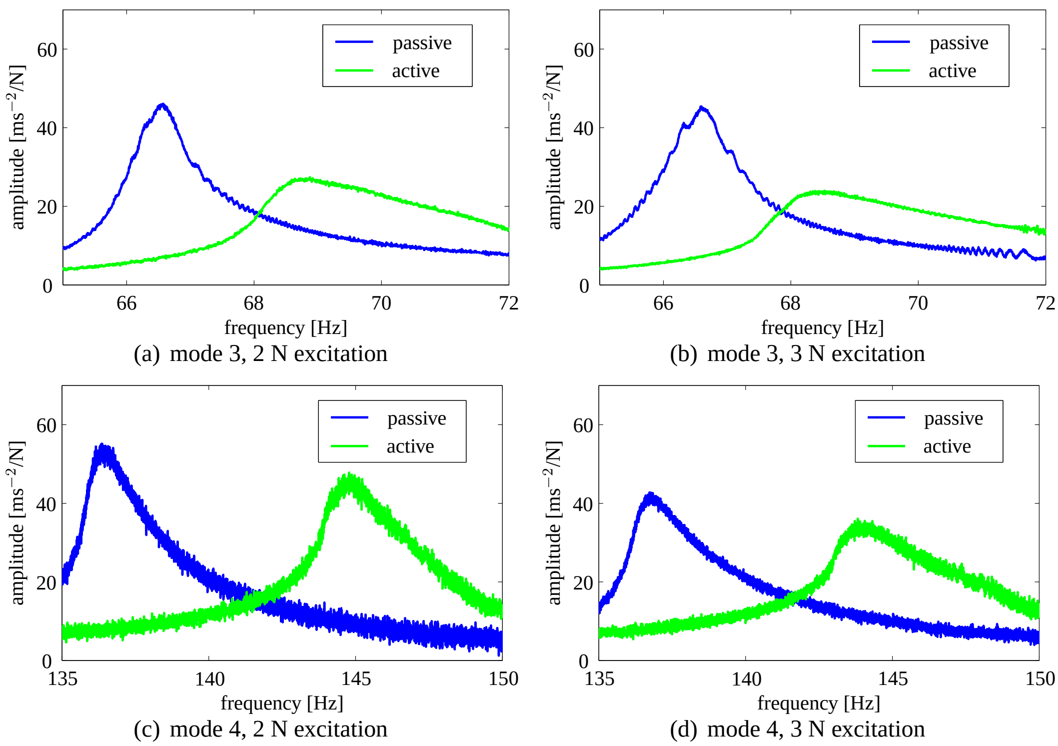

Figure 5: Comparison of measured accelerance FRFs for controlled sine–sweep excitation of different amplitudes with passive damping, i.e. control off, and hysteresis–optimal control.

voltage relation is used instead which is measured for each new configuration or preclamping force during an initialization step. This relation is then used to calculate the required actuator voltage for the prescribed normal force obtained from the Lyapunov–type control law.

3.2 Results

For experimental investigation of the presented control algorithms of the test structure, the parameters for the control laws are determined experimentally and are kept constant for all presented measurements. The multi–modal controllers are compared by measuring accelerance frequency response functions (FRFs). However, for nonlinear mechanical structures such as structures with friction, measuring and comparing FRFs needs special attention. The main obstacle (and difference to linear systems) is the dependence of the obtained (equivalent) eigenfrequencies, the (equivalent) modal damping ratios and hence the peak amplitudes on the vibration amplitude magnitude. Hence, sine sweep measurements of very low speed (0.1 Hz/s) are conducted with controlled excitation force amplitude F_{ext} during the sweep to eliminate the back–EMF effect. Because of the very low sweep speed, the FRFs yield results identical to stepped–sine measurements for the test structure, but the FRFs are recorded for each peak separately due to the large amount of data and long measurement time. The results of Figs. 5 and 6 for example show the accelerance FRFs measured by one accelerometer under control

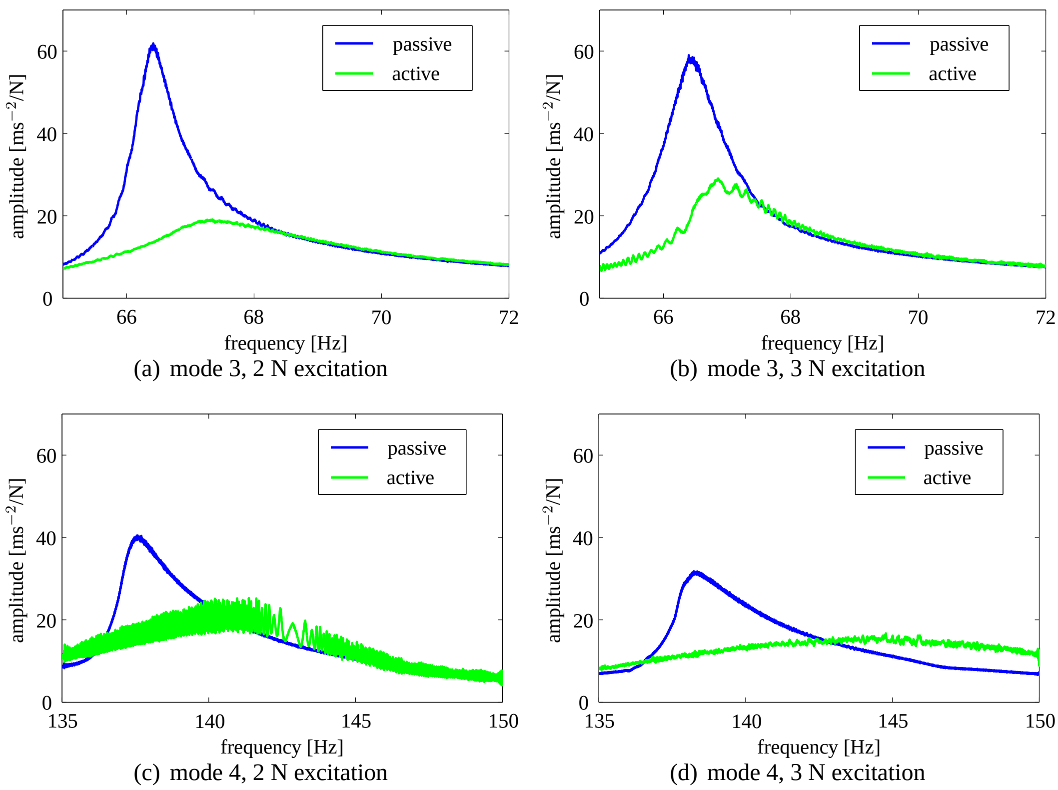

Figure 6: Comparison of measured accelerance FRFs for controlled sine–sweep excitation of different amplitudes with passive damping, i.e. control off, and Lyapunov–type control.

and without control (passive), all accelerometers yield identical results with the only difference that they have different absolute amplitudes due to their individual modal contribution factors. It is seen from the peak widths and the peak amplitudes that the (equivalent) modal damping ratios are strongly increased by the control. Furthermore, the hysteresis–optimal control significantly shifts the resonance amplitudes whereas this effect is only weakly pronounced for the Lyapunov–type control. It is concluded from the experimental results that the Lyapunov–type control is more effective in vibration damping than the hysteresis–optimal control. Even higher damping is achieved by the Lyapunov–type control if a smaller boundary layers ϵ is implemented, but the performance of the excitation amplitude control degrades strongly for certain excitation forces complicating a fair comparison. It is worth mentioning that both controllers do not only increase the normal force but also decreases the normal force below the applied preclamping force if it applies negative voltages to the piezoelectric stack.

Note that the fluctuations observable in the measured FRFs of Fig. 5a can mainly be tracked to the influence of the shaker controller and its interaction with the vibration controller. It is not capable to exactly keep the excitation amplitude constant during the sweep due to the nonlinearities of the structure under control. They can be seen most in FRFs around mode 4 because its nonlinear resonance shift effect is more pronounced than that of mode 3.

4 Conclusion and Outlook

Two control algorithms for semi–active vibration control of structures with friction dampers and normal forces adjustable by piezoelectric actuators are derived and experimentally tested. It is shown that semi–active damping can be very effective in structural vibration damping. The velocity–dependent Lyapunov–type control has its advantage in being the most effective control law, but – contrary to the hysteresis–optimal control – its high output dynamics require high–bandwith high–voltage amplifiers which leads to relatively high power consumption and heat generation depending on the vibration frequency. The hysteresis–optimal control is restricted in theory to mono–frequent vibrations, but can also be implemented with actuators of low dynamics, i.e. actuators of different working principles than piezoelectricity.

In summary, the choice which controller type suits best for a certain application depends mainly on the frequency range of interest, the used force actuator and the type of excitations. In contrast to fully active control methods, semi–active control is fail–safe and guaranteed stable, i.e. significant passive damping is always present in the mechanical system and wrong parameterization can not destabilize the system.

5 Acknowledgment

The support of the DFG with the project SPP 1156 is grateful acknowledged.

References

[1] M. Balas, *Feedback control of flexible systems*, IEEE Transactions on Automatic Control, 23(4), 1978, 673–679.

[2] C. Fuller, S. Elliott, P. Nelson, *Active Control of Vibration*, Academic Press, 1996.

[3] J. S. Lane, A. A. Ferri, B. S. Heck, *Vibration control using semi-active friction damping*, in *Proceedings of the ASME*, vol. 49, 1992, 165–171.

[4] R. Nitsche, L. Gaul, *Lyapunov design of damping controllers*, Archive of Applied Mechanics, 72, 2003, 865–874.

[5] W. N. Patten, C. Mo, J. Kuehn, J. Lee, *A primer on design of semiactive vibration absorbers (sava)*, ASCE Journal of Engineering Mechanics, 124(1), 1998, 61–68.

[6] F. Nitzsche, D. G. Zimcik, V. K. Wickramasinghe, C. Yong, *Control laws for an an active tunable vibration absorber designed for rotor blade damping augmentation*, Aeronautical Journal, 108(1079), 2003, 35–42.

[7] L. Gaul, R. Nitsche, *Role of friction in mechanical joints*, Applied Mechanics Reviews, 54, 2001, 93–105.

[8] L. Gaul, J. Lenz, *Nonlinear dynamics of structures assembled by bolted joints*, Acta Mechanica, 125, 1997, 169–181.